A 3D NUMERICAL FEM MODEL FOR THE SIMULATION OF INDUCTION WELDING OF TUBES

F. Dughiero[(1)], M. Forzan[(1)], M. Garbin[(1)], C. Pozza[(1)], E. Sieni[(2)]

[(1)] University of Padua, Department of Electrical Engineering,
Via Gradenigo, 6/A., 35131 Padova (Italy), E-mail: fabrizio.dughiero@unipd.it
[(2)]Inova Lab srl, Via Torino, 213, 10040 Leinì (Italy)

ABSTRACT. In the present paper, two simulation strategies for tube induction welding process are presented. Coupled electromagnetic and thermal problem is solved by applying three-dimensional FEM models. The resulting power density and temperature distribution are compared. Reported strategies can be used to design tube induction welding devices and to verify the influence of the main parameters of the process, i.e. welding velocity, frequency, specific and total power.

INTRODUCTION

The problem of evaluating the parameters of an induction welding process in order to maximize the performance of the installation and the weld quality is very difficult because of the number of parameters and the complexity of the process itself. In fact, the “vee” shape and position, the welding speed, the tube outer diameter and thickness, the material, frequency and power are only few of the main parameters that can affect the quality of the process [1]- [2].

Up to now, only few general papers have been published on this topic but only one or two are dedicated to the modeling of the process. Moreover, some of these papers deal with 2D very simplified models [3],[4].

In the present paper, 3D FEM models have been applied for the simulation of both electromagnetic and thermal problems in induction welding of tubes. Only non-magnetic materials will be taken into consideration in order to avoid the difficulty in terms of time and memory requirements for the solution of real non-linear problems.

The electromagnetic problem has been solved by a complete A-V formulation in order to calculate the power density distribution inside the tube thickness. Starting from the power density distribution, a simplified model is used for the calculation of the temperature values in the most important region of the welded joint, i.e. close to the welding edges.

DESCRIPTION OF THE PROBLEM

During the welding process, the tube is moving with velocity v_t, in a time varying magnetic field, H. In order to evaluate the temperature at the welding point, a magneto-thermal problem coupled with a translation movement has to be solved. Maxwell equations are solved considering skin and proximity effects on current density distribution in order to compute the power density induced in the tube by the magnetic field. The computation of the magnetic

flux density and the induced current density across the tube section and in the surrounding air is obtained by solving a time-harmonic eddy current problem at the welding frequency.

Usually, frequencies involved in tube welding process are between 100 and 450 kHz [2], [5], a range where Maxwell equations can be solved in the quasi-stationary case. Finally, a transient thermal analysis is carried out to evaluate the temperature distribution.

FORMULATION

The electromagnetic (EM) problem has been solved in terms of the phasor of the magnetic vector potential, $\dot{\bar{A}}$, and the phasor of the electric scalar potential, $\dot{V}$. Since eddy currents are concentrated close to welding edges, only the part of tube close to the coil (figs. 1 and 2) has been considered in the simulation. In particular, the non-homogeneous Helmholtz equation is solved in the tube region Ω_T (fig. 2):

$$\nabla^2 \dot{\bar{A}} + k^2 \dot{\bar{A}} = -\mu \dot{\bar{J}}, \quad k^2 = -j\omega\mu\sigma \tag{2}$$

where μ and σ are, respectively, the magnetic permeability and the electric conductivity of the materials, and the Lorentz gauge has been imposed [6], [7].

In the tube region Ω_T, modelled as a conductive region, the current density is computed from the magnetic vector potential and the electric scalar potential by means:

$$\dot{\bar{J}} = \sigma \dot{\bar{E}} = -\sigma(j\omega \dot{\bar{A}} + \nabla \dot{V}) \tag{3}$$

where $\dot{\bar{E}}$ is the phasor of the electric field.

Since the air regions, Ω_A and Ω_{BOX}, are not conductive regions, $\dot{\bar{J}}$ and k^2 in (2) are set to zero, and the EM problem is solved only in terms of vector potential $\dot{\bar{A}}$. The magnetic field source consists of two turns with an impressed current. At the domain boundary, Ω_{INF}, infinite boundary conditions are imposed in order to set the magnetic vector potential to zero at infinite distance.

The temperature distribution across the tube section can be evaluated by solving the Fourier equation of the thermal problem in the tube region Ω_T [8]:

$$c\gamma \frac{\partial T}{\partial t} = \lambda \nabla^2 T + p \tag{4}$$

where the power density p is computed from the previous electromagnetic solution, λ is the thermal conductivity [$W \cdot m^{-1}K^{-1}$], c is the specific heat [$J \cdot kg^{-1}K^{-1}$] and γ is the mass density of the material [$kg \cdot m^{-3}$].

The tube is supposed to be at room temperature at the beginning of the welding process (T = 293.15 K). At the tube surface, suitable heat exchange conditions are imposed. In particular, the region around the tube is at 293.15 K. Convection and radiation are considered for both inner and outer tube surface, as well as the welding edge.

Electric and thermal characteristics of the materials are reported in Table I and Table II, while thermal model characteristics are reported in Table III.

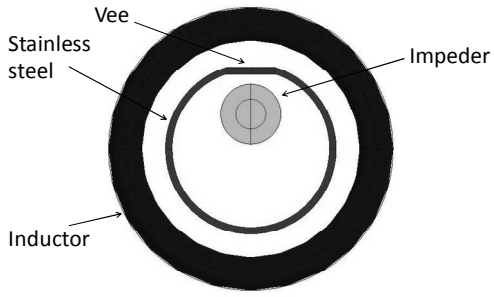

Figure 1. Model geometry of the welding system.

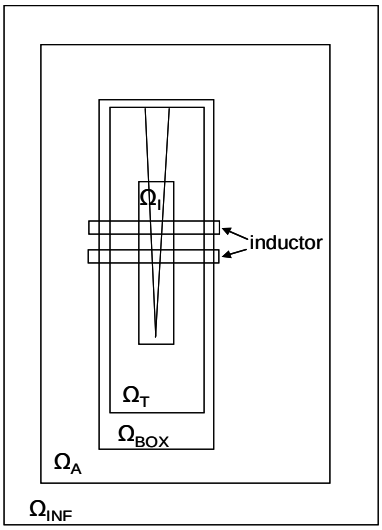

Figure 2. Different regions in the model geometry.

Table I. Electric characteristics of materials.

Material	ρ [Ωm]	μ_r
Stainsless steel	$120 \cdot 10^{-8}$	1
Air	10^6	1
Impeder	--	40

Table II. Thermal characteristics of materials. T is the temperature in [K].

Material	λ [W m^{-1} K^{-1}]	c [J kg^{-1} K^{-1}]	Density [kg m^{-3}]
Stainless steel	See fig. 3	See fig. 4	8000
Air	0.03	1300	0.03

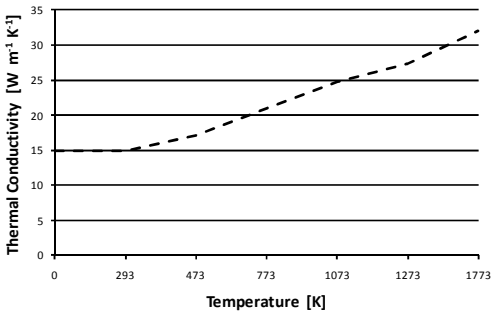

Figure 3. Thermal conductivity vs. temperature.

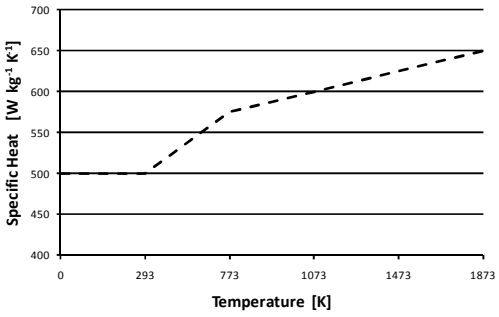

Figure 4. Specific heat vs. temperature.

Table III. Thermal model characteristics.

Type of Surface	Emissivity	Convection [Wm^{-2}K^{-1}]
External	0.7	12
Internal	0.7	12
Welding edge	0.7	10

SIMULATION STRATEGY

The purpose of this study is to solve a thermal and EM coupled problem taking into account the movement of the tube. In fig. 5, a simplified geometry of the tube and welding coil is sketched; the strip is moving through the coil, while the welding point remains at a fixed distance from the inductor as in fig. 6. At the same time, the bending of the strip by the welding rolls causes a gradual approaching of the welding edges. Unfortunately, the simulation tool cannot manage simultaneous movements along two different directions. Then, two simulation strategies have been developed to avoid this issue and to compute the power density and temperature distribution in the welding region.

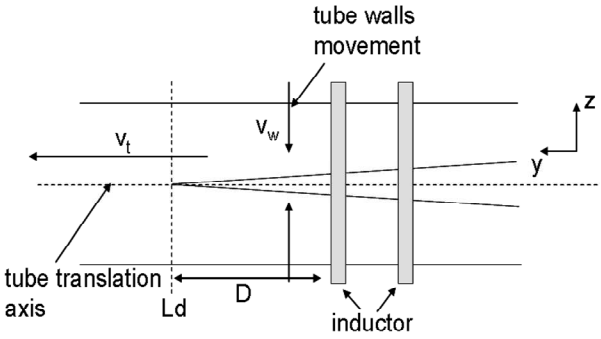

Figure 5. Tube movement directions

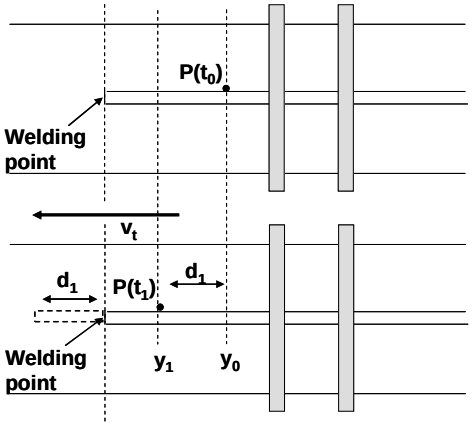

Figure 6. Welding process

The first strategy is based on an equivalent-energy approach, while, in the second one, an analysis of the entire magneto-thermal transient is performed.

STRATEGY 1: EQUIVALENT ENERGY BASED APPROACH

Geometry

The geometry of the EM model is sketched in Figs. 1 and 7 in front and longitudinal views. The system is composed by a stainless steel tube and a welding coil. The welding coil consists in two series-connected turns, supplied by a 1800 A_{rms} /190 kHz AC current. Furthermore, an impeder, made of a soft magnetic material, is placed inside the tube. The air region is surrounded by an infinite region.

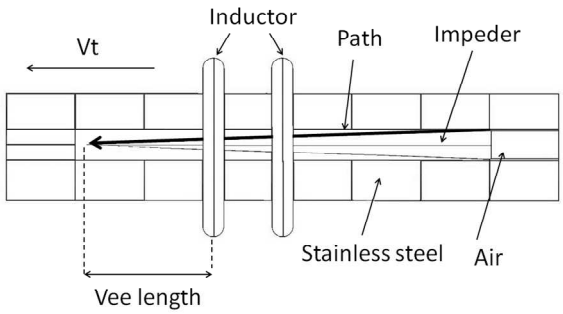

Figure 7. Geometry adopted in the first strategy model.

To avoid some issues deriving from data exportation, a simplified EM model with parallel welding edges (fig. 8) is used. It is divided into N annular elements of height H_T, where H_T must be carefully chosen because it strongly affects the precision of the computation. One of the annular elements is then used as the geometry of the thermal model (Figs. 8 and 9).

The EM and thermal problems have been solved using a commercial Finite Element Method (FEM) tool [9]. In the realistic EM model, the first-order mesh is composed by 160000 nodes and 950000 volume elements, whereas the simplified EM model consists of 100000 nodes and 650000 volume elements. The thermal model is discretized with 330000 nodes and 430000 volume elements.

Description of the Strategy 1

The problem is solved by following an equivalent-energy-based strategy. First, the power density distribution $p(y)$ is evaluated along a y path on the welding edge in the realistic EM model, as in figs. 7 and 10.

Since the tube is moving at constant velocity, the considered cross section has been subjected to an average power density passing from the initial position y_0 to the position y_i, that can be defined as:

$$\prec p \succ = \frac{\int_{y_o}^{y} p(y) \cdot dy}{y_i - y_0} \tag{5}$$

Referring to the simplified EM model in fig. 8, it is possible to evaluate a new power density distribution $p_{aux}(y_{aux})$ along a similar path on the welding edge, and to find the position $y_{i,aux}$ along that path, so that $p_{aux}(y_{i,aux}) = \prec p \succ$. The power density distribution on the slice corresponding to the position $y_{i,aux}$ is used as equivalent thermal source in the thermal model to compute the temperature increase. Thus, the temperature distribution on any cross section along the tube can be easily obtained.

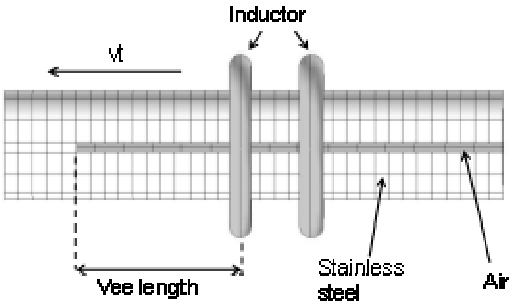

Figure 8. Simplified EM model in the first strategy.

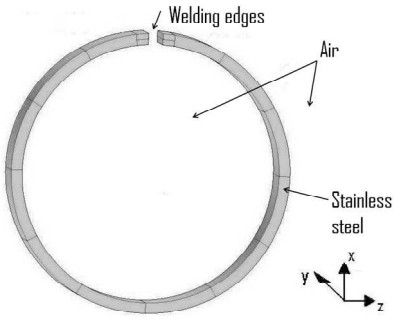

Figure 9. Thermal model in the first strategy.

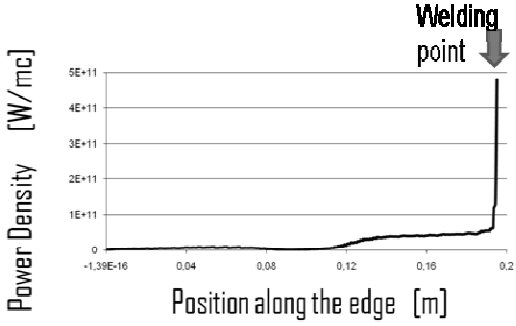

Figure 10. Power density distribution along the welding edge.

STRATEGY 2: TRANSIENT ANALYSIS

Geometry

The geometry of the model for the EM simulation is sketched in Figs. 2 and 11, where regions used in simulation are defined. The stainless steel tube Ω_T is a conductive non ferromagnetic region, with parallel welding edges, and the welding coil is the magnetic field source. The impeder inside the tube is modelled as a magnetic region Ω_I. The tube, the impeder and the coil are surrounded by the air regions, Ω_A and Ω_{BOX}. The Ω_{BOX} region is used to facilitate the re-meshing of the domain. At the domain boundary, the infinity region, Ω_{INF}, is placed. Initial and boundary conditions are imposed as well as in the first strategy models.

The EM and thermal problems have been solved using a commercial Finite Element Method (FEM) tool [9]. The mesh is a first-order mesh with 270000 nodes and 1000000 volume elements.

Description of the Strategy 2

The temperature is computed solving an EM problem coupled with a transient thermal and mechanical problem. Since the welding point is fixed in space, as in fig. 11, a demarcation line *Ld* can be introduced in the model. The region Ω_W changes its electric and thermal properties from the ones of an air region to the ones typical of a steel, in every point that crosses the line *Ld* during the tube translation. In this way, the volume region of the tube follows a translational movement that develops along only one direction.

At each time step, the power density distribution throughout the tube, obtained from the solution of the EM problem, is used as thermal source in the thermal problem. Then, the tube region is displaced along the longitudinal direction as in fig. 11, to perform the mechanical step. Final power density and temperature distributions are obtained when the tube reaches a stationary thermal regime.

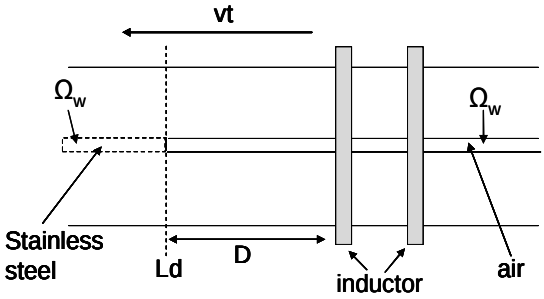

Figure 11. Model geometry of the tube.

RESULTS

Figs. 12-13 show results of the EM and thermal analysis, respectively, obtained from the first strategy. It can be noticed that skin and proximity effects are considered and the heat affected zone is close to welding edges. Then, the welding edge temperature reaches the melting temperature at the welding point.

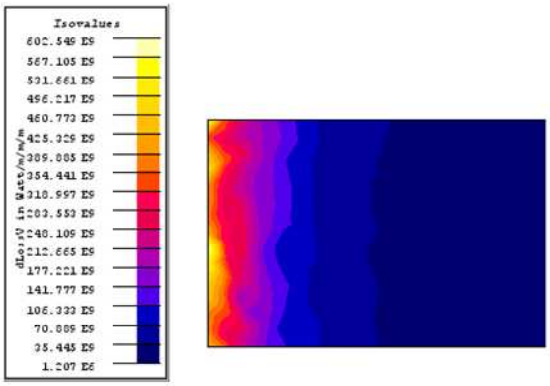

Figure 12. Power density distribution on the tube cross section at the welding point (first strategy).

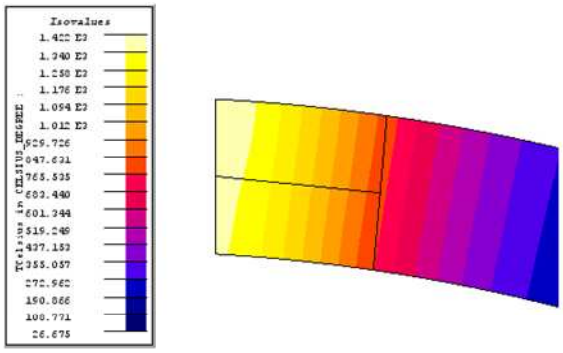

Figure 13. Temperature distribution on the tube cross section at the welding point (first strategy).

Figs. 14-15 show power density and temperature distributions obtained with the second strategy. Skin and proximity effects are considered, although some inaccuracies are introduced because welding edges are considered to be parallel for all the tube length. Even in this case, the temperature increases along the welding edge and reaches the melting temperature at the welding point.

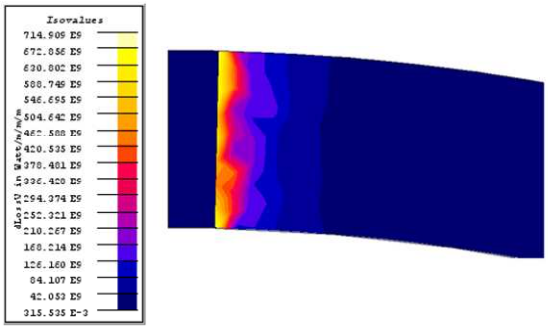

Figure 14. Power density distribution on the tube cross section at the welding point (second strategy).

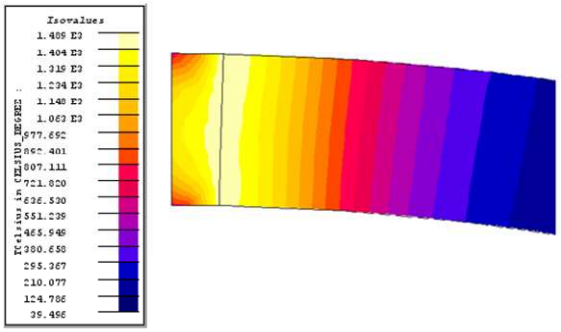

Figure 15. Temperature distribution on the tube cross section at the welding point (second strategy).

The power density and temperature distribution along the welding edge for the two strategies are compared in figs. 16-17.

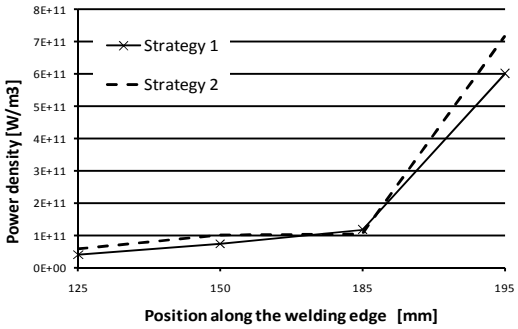

Figure 16. Power density in the tube for the first and second strategy models, respectively, as a function of the position on the welding edge.

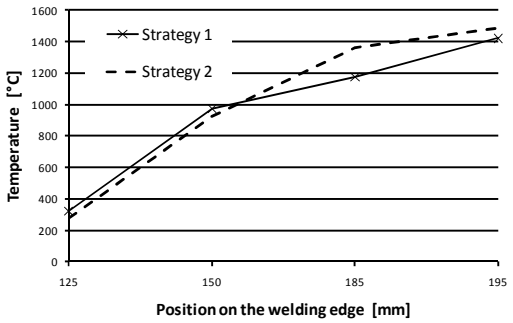

Figure 17. Temperature distribution on the welding edge for the first and second strategy models, respectively, as a function of the position on the welding edge.

CONCLUSIONS

A comparison of the results obtained by means of two different strategies for the evaluation of power density and temperature distributions close to the welding edges has been carried out. Both the approaches provide comparable results, in terms of power density distribution, and as regards the temperature distribution; the EM and thermal problems are correctly solved by both strategies.

The first strategy allows the direct calculation of the final temperature distribution, but many inaccuracies are introduced, such as the hypothesis of constant resistivity. Furthermore, temperature distribution beyond the welding point is not calculated.

The second strategy gives more accurate results, since the material properties can vary point to point. However, computational costs are very important and become prohibitive when the simulated system is characterized by long time constants.

Results will be verified by future tests, even if both the strategies show good agreement with experimental data available in literature.

REFERENCES

[1] Kim, H.J., Youn, S.K. (2008). Three Dimensional Analysis of High Frequency Induction Welding of Steel Pipes With Impeder, *J. Manuf. Sci. Eng*., vol. 130, 031005.

[2] Scott, P.F.. The Effects of Frequency in HF Welding, *www.thermatool.com.*

[3] Buser, J., Asperheim, J.I., Grande, B., Markegard, L., Lombard, P. (1998). Computation and analysis of temperature distribution in the cross-section of the weld Vee, *Tube International*.

[4] Asperheim, J. I., Grande, B. (2000). Temperature Evaluation of Weld Vee Geometry and Performance, *Tube International,* Vol. 19, no. 110, 497-502.

[5] Scott, P.F. (1996). Key Parameters of High Frequency Welding, *www.thermatool.com*

[6] Marechal, Y., Meunier, G., Ben Harara, H. (1992). A new 3D AV- ϕ - ϕ formulation, *IEEE Trans. Magn.*, Vol. 28, 1204–120.

[7] Morisue, T. (1993). A Comparison of the Coulomb gauge and Lorentz gauge magnetic vector potential formulation for 3D eddy current calculations, *IEEE Trans. Magn.*, Vol. 29, 1372–1375.

[8] Carslaw, H.S., Jaeger, J.C. (1959). Conduction of heat in solids, *Clarendon Press*, Oxford.

[9] CEDRAT, http://www.cedrat.com, FLUX users guide.